



Structure of the Na,K-ATPase regulatory protein FXYP2b in micelles: Implications for membrane–water interfacial arginines[☆]

Xiao-Min Gong, Yi Ding, Jinghua Yu, Yong Yao, Francesca M. Marassi^{*}

Sanford-Burnham Medical Research Institute, 10901 North Torrey Pines Road, La Jolla, CA 92037, USA

ARTICLE INFO

Article history:

Received 26 February 2014

Received in revised form 19 April 2014

Accepted 23 April 2014

Available online 2 May 2014

Keywords:

FXYP

membrane protein

structure

NMR

Na

K-ATPase

ABSTRACT

FXYP2 is a membrane protein responsible for regulating the function of the Na,K-ATPase in mammalian kidney epithelial cells. Here we report the structure of FXYP2b, one of two splice variants of the protein, determined by NMR spectroscopy in detergent micelles. Solid-state NMR characterization of the protein embedded in phospholipid bilayers indicates that several arginine side chains may be involved in hydrogen bond interactions with the phospholipid polar head groups. The structure and the NMR data suggest that FXYP2b could regulate the Na,K-ATPase by modulating the effective membrane surface electrostatics near the ion binding sites of the pump. This article is part of a Special Issue entitled: NMR Spectroscopy for Atomistic Views of Biomembranes and Cell Surfaces. Guest Editors: Lynette Cegelski and David P. Weliky.

© 2014 Elsevier B.V. All rights reserved.

1. Introduction

The critical balance of Na⁺ and K⁺ ion concentrations across cell membranes is maintained primarily by the Na/K-ATPase, an integral membrane enzyme complex that hydrolyses intracellular ATP to generate the energy required to exchange three Na⁺ ions for two K⁺ ions across the plasma membrane [1–3]. The enzyme's activity is regulated by its three subunits – a catalytic α subunit, an auxiliary β subunit and a regulatory γ subunit, also known as FXYP protein due to a conserved amino acid sequence in its N-terminus. The expression of FXYP genes is tissue-specific, cell-specific and developmentally regulated. The proteins are prevalent in the early stages of fetal life, in tissues that specialize in fluid or solute transport or that are electrically excitable. Their association with the Na,K-ATPase induces specific changes in the enzyme's kinetics and affinity for Na⁺, K⁺ and ATP [3–6]. Several FXYP family members have been linked with major human diseases, including heart failure (FXYP1) [7], hypomagnesemia (FXYP2) [8], cancer (FXYP3, FXYP5) [9,10], and schizophrenia (FXYP6) [11], and represent attractive targets for therapeutic development.

Although the FXYP proteins typically possess a single transmembrane helix and are relatively small, they are all encoded by genes with as many as nine exons [5]. Interestingly, the protein structures mirror the intron–exon arrangements of their corresponding genes, suggesting that discrete structured domains may have evolved to confer

different functional properties in various physiological settings [12]. The family members share a core homology of 35 conserved amino acids, in and around a single transmembrane segment (Fig. 4A). The short signature motif, PFXYP (Pro, Phe, X, Tyr, Asp) is highly conserved in all known mammalian proteins, with residue X usually occupied by Tyr, but also Thr, Glu, or His. Conserved basic residues flank the transmembrane region, the extracellular N-termini are acidic, and the cytoplasmic C-termini are basic. However, outside of this homology region there is little sequence conservation among the family members. The distinct functionalities of FXYP proteins on the Na,K-ATPase's rate constant and affinities for Na⁺, K⁺ and ATP are largely ascribed to differences in their cytoplasmic domains, whose sequences vary widely among the family members.

FXYP2, the first FXYP protein to be identified as an accessory component of the Na,K-ATPase [13,14], inhibits the activity of the pump by increasing its apparent affinity for both Na⁺ and K⁺ [15–20]. Its function is modulated by post-translational modification [16,18], as well as by gene splicing and RNA editing, which respectively govern the expression of two splice variants, FXYP2a and FXYP2b, and of a truncated form of FXYP2b that is not exported to the plasma membrane [5,13,14,21]. The two splice variants of FXYP2 have identical amino acid sequences, except in their N-terminal segments, encoded by the first exon [22, 23]. Both FXYP2a and FXYP2b are expressed primarily in kidney, albeit in distinct nephron segments, with FXYP2a in proximal and FXYP2b distal convoluted tubules [23–26]. The function of FXYP2 has been implicated in embryonic development [27], while misrouting of the protein due to the Gly41Arg mutation in the transmembrane segment has been linked with familial hypomagnesemia, a disease characterized by renal or intestinal Mg²⁺ loss [8]. The transmembrane span of FXYP2

[☆] This article is part of a Special Issue entitled: NMR Spectroscopy for Atomistic Views of Biomembranes and Cell Surfaces. Guest Editors: Lynette Cegelski and David P. Weliky.

^{*} Corresponding author. Tel.: +1 858 795 5282; fax: +1 858 713 6268.

E-mail address: fmarassi@sbmri.org (F.M. Marassi).

has been implicated in modulation of the Na,K-ATPase's affinity for Na⁺ [28], while the N- and C-termini have been implicated in modulation of the Na⁺ and K⁺ affinities [25].

The first crystal structure, determined for pig kidney Na,K-ATPase confirmed that FXYP2 is an integral component of the enzyme complex and showed that its transmembrane helix associates with α M9, the ninth transmembrane helix of the α subunit [29]. The α -FXYP association is stabilized by the amino acid sequence of α M9, which is highly conserved among all α subunit isoforms [4], and by a set of highly conserved FXYP protein residues (Gly28, Gly33, Phe36 and Gly39 in FXYP2b) that form a distinctive “notch-peg-notch” shape along the helix length [30]. This intimate α -FXYP transmembrane association is also observed in the more recent crystal structure of Na,K-ATPase from pig kidney [31–34] and from shark [35,36], and may be important for modulating the activity of the enzyme's Na⁺ binding sites [33].

The signature FXYP motif has been proposed to adopt an extended hook-like conformation that stabilizes the extracellular region of the β chain through hydrogen bond and salt bridge contacts [34–36]. However, the extramembrane regions of the FXYP and β chains are incompletely and/or poorly defined by the electron densities in the crystal structures of Na,K-ATPase. The NMR structures of FXYP1 and FXYP4, determined in micelles, separate from the Na,K-ATPase complex, show that the FXYP motif adopts a short loosely helical conformation in FXYP1 and a long well-formed helix in FXYP4 [30,37]. In both structures, the transmembrane helix is followed by a short helical extension of conserved basic residues that anchor it near the membrane–water interface, and a ~10-residue amphipathic C-terminal helix that associates with the membrane surface. This helix contains the phosphorylation sites of FXYP1 and could modulate the electrostatic potential at the membrane surface, near the Na⁺/K⁺ ion binding sites of the Na,K-ATPase α subunit [38].

Here we describe the NMR structure of FXYP2b determined in micelles. Solid-state NMR data, obtained for FXYP2b in magnetically aligned lipid bilayers, reflect the transmembrane orientation of the protein and show that several arginine side chains are immobilized, possibly due to hydrogen-bonded interactions with the phospholipid polar head groups. Such interactions could contribute to the membrane surface electrostatics and assist the recruitment of specific negatively charged phospholipids important for Na,K-ATPase stability and function.

2. Materials and methods

2.1. Sample preparation

Human FXYP2a and FXYP2b were prepared as described previously [39]. Briefly, the proteins were each expressed as C-terminal fusions to His₉-Trp Δ LE-Met, purified by Ni-affinity chromatography and then separated from the fusion partner by CNBr chemical cleavage. Two mutations Met1Leu and Cys50Ser (in FXYP2b) or Cys52Ser (in FXYP2a) were introduced to facilitate cleavage and purification. Uniform ¹³C/¹⁵N isotopic labeling was obtained by supplementing minimal M9 growth media with ¹³C-glucose and (¹⁵NH₄)₂SO₄ (Cambridge Isotope Laboratories, Andover, MA).

Samples for solution NMR spectroscopy were prepared by dissolving pure lyophilized protein in 300 μ L of buffer (20 mM sodium citrate at pH 5, 10 mM DTT, 10% D₂O) containing 500 mM sodium dodecyl sulfate (SDS) or 150 mM dodecyl-phosphocholine (DPC). For residual dipolar coupling (RDC) measurements, the samples were weakly aligned in 6.5% polyacrylamide gels by means of vertical compression, as described previously [12].

Magnetically aligned lipid bilayer samples for solid-state NMR spectroscopy were prepared by dissolving 2–3 mg of pure lyophilized protein in 1,2-O-diethyl-sn-glycero-3-phosphocholine (6-O-PC) and then adding the resulting solution to a dispersion of the longer chain lipid 1,2-O-ditetradecyl-sn-glycero-3-phosphocholine (14-O-PC) to obtain a molar ratio 3.2 for long-chain to short-chain lipid. The final

sample, containing 300 mM 14-O-PC in a volume of 180 μ L at pH 6.7, was transferred to a flat-bottomed, 5 mm outer diameter NMR tube (New Era Enterprises, Vineland, NJ) for NMR studies.

2.2. NMR experiments

Solution NMR experiments were performed at 40 °C on a Bruker AVANCE 600 MHz spectrometer equipped with a ¹H/¹⁵N/¹³C triple-resonance cryoprobe. Solid-state NMR experiments were performed on a Bruker AVANCE 500 MHz spectrometer with a home-built ¹H/¹⁵N double-resonance 5 mm solenoid coil probe. The NMR data were processed using NMRPipe [40] and analyzed using Sparky [41].

The ¹H/¹⁵N/¹³C two- and three-dimensional solution NMR experiments, for backbone resonance assignments, measurements of resonance intensity and RDC measurements, were performed as described previously for FXYP1 [30]. Chemical shifts were referenced to the H₂O resonance set to its expected position at 40 °C [42]. Dihedral angles were derived from analysis of the NMR chemical shifts with the program TALOS+ [43]. The ¹H/¹⁵N one- and two-dimensional oriented sample (OS) solid-state NMR experiments were performed as described previously [44].

To probe the association of FXYP2b with the micelle environment, we examined the paramagnetic relaxation enhancement (PRE) broadening effect of Mn²⁺ on the ¹H/¹⁵N HSQC spectrum of the protein. PRE restraints were obtained by measuring the resonance intensities in the ¹H/¹⁵N HSQC spectrum of FXYP2b after addition of increasing amounts of 1.8 mM MnCl₂ to the micelle solution.

2.3. Computational methods

Structure calculations were performed with XPLOR-NIH [45,46]. The structure coordinates and NMR restraints have been deposited in the

Table 1
NMR structure statistics for FXYP2b.

Number of experimental NMR restraints	
Dihedral angles	
phi	38
psi	38
Residual dipolar couplings (RDC)	
¹ H– ¹⁵ N RDC	60
Distances	
CO–HN hydrogen bonds	38
Plane distances	
HN–plane	8
Structure statistics ^a	
Violations (mean \pm s.d.)	
Dihedral angle restraints (°)	1.145 \pm 0.111
¹ H– ¹⁵ N RDC restraints (Hz)	0.767 \pm 0.029
Distance restraints (Å)	0.144 \pm 0.003
Plane distance restraints (Å)	1.311 \pm 0.087
Deviations from idealized geometry	
Bond lengths (Å)	0.002 \pm 0.000
Bond angles (°)	0.461 \pm 0.008
Improper (°)	0.460 \pm 0.011
Average pairwise r.m.s.d. (Å)	
Backbone	0.181 \pm 0.059
Heavy	1.038 \pm 0.106
Ramachandran plot statistics ^b	
Residues in most favored regions (%)	86.3
Residues in additional allowed regions (%)	11.2
Residues in generously allowed regions (%)	2.2
Residues in disallowed regions (%)	0.4

^a Evaluated for 10 lowest energy structures out of a total 100 calculated structures.

^b Evaluated with the program PROCHECK [49].

Protein Data Bank (PDB ID: 2MKV) and structure statistics are reported in Table 1.

Two conventional simulated annealing protocols were used [47], the first for folding 100 structures from an initially extended conformation and the second for subsequent refinement of 100 structures from the lowest energy structure of the first protocol. Experimental restraints included dihedral angles derived from chemical shifts, hydrogen bond distances derived from $^1\text{H}/^2\text{H}$ exchange, and amide NH bond orientations derived from RDCs (Table 1). The knowledge-based statistical torsion angle potential torsionDB was implemented as described previously [47].

Plane distance restraints, derived from the Mn^{2+} PRE data, were implemented in the refinement stage, using the plane distance potential recently developed for XPLOR-NIH [48], instead of the harmonic coordinate plane restraints that we used previously for structure determination of FXYP1 [30]. Based on the data, backbone N atoms from residues Trp4, Tyr5 and Leu29 were restrained to one common plane representative of the extracellular membrane surface, and N atoms from Lys55–Arg57 and Ser50 were restrained to another plane representative of the cytoplasmic surface. The planes were defined to be perpendicular to the long axis of the transmembrane helix and the plane distance restraints were implemented loosely (± 3 Å).

3. Results and discussion

3.1. Structure of FXYP2b in micelles

The structure of human FXYP2b is shown in Fig. 1. The transmembrane helix (h2), spanning residues Gly27–Leu44, is clearly defined by backbone amide hydrogens that are protected from exchange with bulk water (Fig. 2A). As observed in the structures of human FXYP1 and rat FXYP4 [30,37], a set of conserved amino acids form a long groove parallel to the length of the transmembrane helix, delineating the binding interface with the Na,K-ATPase αM9 helix. The groove is lined by conserved glycines (Gly28, Gly33, Gly39) and interrupted by the aromatic ring of Phe36, which protrudes from the transmembrane helix like a key ready to engage its lock. Helix h2 is preceded by a short helical segment (h1) that spans residues Phe17–Arg25 and includes the FXYP signature motif (FYYP in FXYP2).

A short helix (h3), spanning residues Ser45–Ser50, extends beyond the hydrophobic portion of the transmembrane helix and contains the

conserved arginine-rich sequence RRFR of the protein. Helices h2 and h3 of FXYP2b form a single extended transmembrane helix, while those of FXYP1 and FXYP4 are separated by a kink that changes helix direction slightly. Furthermore, FXYP2b lacks the well-defined cytoplasmic amphipathic helix observed in FXYP1 and FXYP4, and has somewhat less structural order in this region. Beyond the helical regions, the backbone of extracellular Trp4, Tyr5 and Leu6 and cytoplasmic Lys55, Arg56, and Arg57 associate with the micelle–water interface.

Overall, helices h1, h2, and h3 have similar backbone dynamics, with similar values of $^1\text{H}/^{15}\text{N}$ heteronuclear NOEs (Fig. 2B), order parameters (Fig. 2C) and $^1\text{H}/^{15}\text{N}$ HSQC peak intensities (Fig. 3B). Notably, residues Trp4–Gly7 in the N-terminus of the protein and residues Lys55–Arg57 in the C-terminal cytoplasmic region, also exhibit restricted dynamics, while Pro10–Pro16 and the C-terminus are significantly more flexible, with negative values of the $^1\text{H}/^{15}\text{N}$ NOE and greater peak intensities.

FXYP2a, the longer splice variant, is structurally similar to FXYP2b, as evidenced by the similarity of their HSQC cross peak chemical shifts (Fig. 3A). Significant chemical shift changes are observed only in the N-termini where the amino acid sequences of the two proteins differ (Fig. 3C). Notably, however, the slightly longer N-terminus of FXYP2a is significantly more dynamic all the way to Gly14, as evidenced by much greater HSQC peak intensities (Fig. 3B). This feature could be important for the different physiological functions of FXYP2a and FXYP2b.

In FXYP2b, the FYYP-spanning helix is oriented at a $\sim 90^\circ$ angle from the transmembrane helix. The arrangement of the FYYP motif helix relative to the micelle–water interface is consistent with the propensity of Phe and Tyr to associate with lipids. By contrast, the FXYP motifs of shark FXYP10 and pig FXYP2 have been proposed to adopt an extended hook-like structure forming extensive interactions with the extracellular regions of the β subunit of their respective Na,K-ATPase [34–36]. These regions of the complex are incompletely and/or poorly defined by the crystallographic data, especially in the case of pig kidney Na,K-ATPase containing FXYP2 [29,31–34]. However, it is possible that the extramembrane regions of FXYP proteins adopt different structures in their isolated states separate from the Na,K-ATPase complex. Several studies indicate that FXYP proteins can exist separately from the Na,K-ATPase [50] and associate with different partners, including the $\text{Na}^+/\text{Ca}^{2+}$ exchanger and some Ca^{2+} channels [51,52]. The NMR data for FXYP2b (Fig. 2B) and other FXYP proteins [30,37,38,53] are

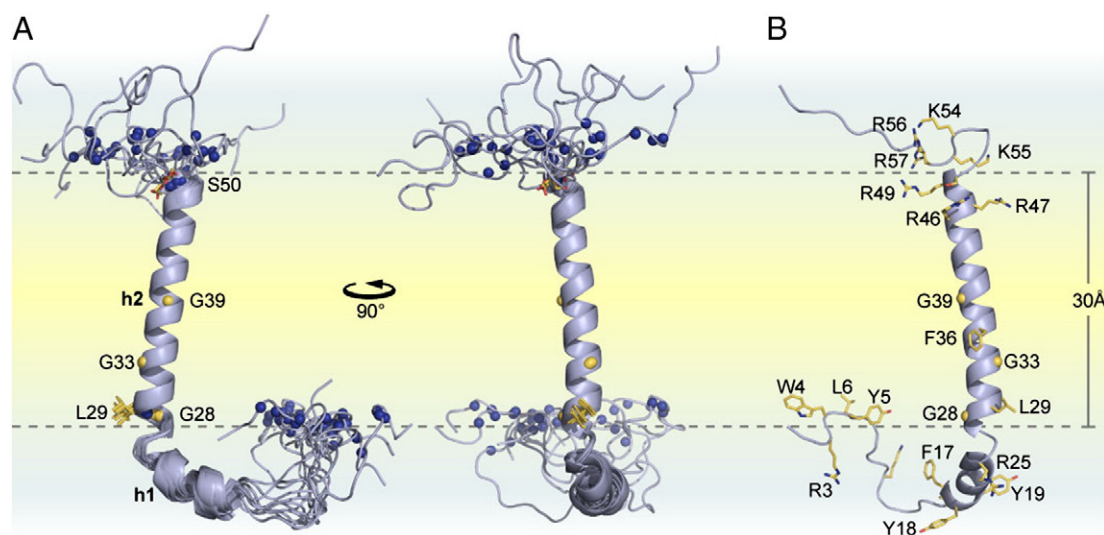


Fig. 1. Structure of FXYP2b determined in micelles. (A) Orthogonal views of the ten lowest energy NMR structures. Amide N atoms whose positions were restricted by plane distance restraints, derived from the Mn^{2+} PRE data, are shown as blue spheres. The two planes coincide with the micelle–water interface and each contain the amide N atoms of L29 or S50. (B) Lowest energy structure of FXYP2b showing side chains for arginines and other key residues that associate with the micelle interior.

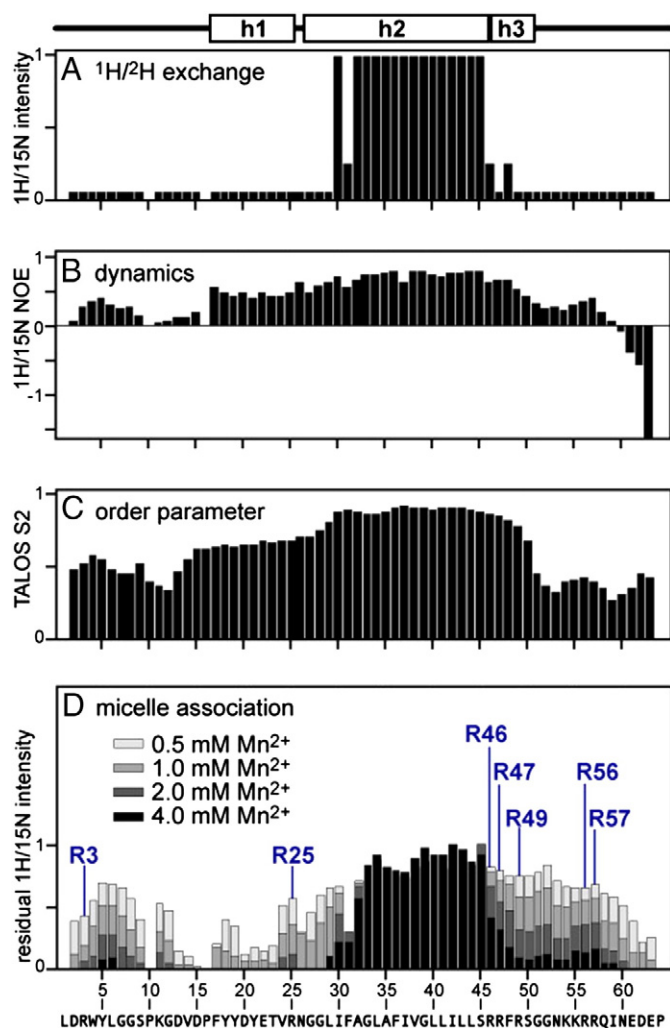


Fig. 2. Summary of structural and dynamic features of FXYD2b in micelles. The helical structure is outlined above the graphs. (A) Amide $^1\text{H}/^{15}\text{N}$ exchange profile. (B) Heteronuclear $^1\text{H}/^{15}\text{N}$ NOEs. (C) Order parameters (S2) derived from TALOS+ analysis of the chemical shifts. (D) Mn^{2+} PRE profile showing residual $^1\text{H}/^{15}\text{N}$ NMR intensity measured after addition of increasing concentrations of MnCl_2 . Peak intensities were measured in the presence of increasing concentrations of Mn^{2+} (see legend). Residual normalized peak intensity is the ratio of the intensity measured without Mn^{2+} to that measured in the presence of Mn^{2+} . Data for the seven Arg backbone sites are labeled.

consistent in showing that the extramembrane regions of FXYD proteins are more dynamic, a property that could enable them to adopt different conformations in different settings or in the presence of their different partners. Structure determination of the whole FXYD protein within the enzyme complex will be needed to understand the precise conformations and functions of the extramembrane regions with respect to Na,K-ATPase regulation.

No conclusive function has been assigned to the signature FXYD sequences. The FXYD motifs of FXYD2 and FXYD10 have been proposed to stabilize the Na,K-ATPase through interactions with the extracellular regions of the α and β chains [34–36]. However, recent data argue against involvement of the FXYD, β and α extramembrane regions in stabilizing the Na,K-ATPase, and instead, attribute the stabilizing influence of the FXYD proteins on the Na,K-ATPase primarily to the FXYD transmembrane helices and to the effects of FXYD proteins in promoting the interactions of the enzyme with specific phospholipids, such as negatively charged phosphatidylserine [54,55]. It is also possible that the FXYD motif helps stabilize the lipid bilayer membrane structure surrounding the enzyme complex and/or constitutes a localization signal.

A BLAST (Basic Local Alignment Search Tool) search of the NCBI protein sequence database, seeded with the short polypeptide sequence DVDPFYD, identifies this sequence in numerous proteins from a wide variety of organisms, including prokaryotes (Fig. 4). Notably, the identification of entire FXYD protein sequences within other multi-domain membrane proteins (identified with TMHMM [56]) further indicates that they can have functions beyond Na,K-ATPase regulation.

Interesting examples include the 2174-residue DSCAM protein (Down syndrome cell adhesion molecule-like protein 1), which contains an entire FXYD protein sequence spanning residues 13–56, the shorter 343-residue DSCAM, which contains two contiguous entire FXYD protein sequences spanning residues 24–67 and 91–137, and the 894-residue serine protease, which also contains an entire FXYD protein sequence from residues 13–56 (Fig. 4B). These may be classified as members of the FXYD family since they share sequence homology across the FXYD motif as well as the conserved features of the transmembrane helix. The FXYD motif is also found in other membrane proteins (Fig. 4C) and several soluble proteins (Fig. 4D) with various functions, including GTP-binding proteins, lipoproteins and ankyrin repeat proteins. Functional insights may be also attained by careful analysis of other FXYD motif containing proteins as their sequences and structures become available in the databases.

3.2. Association of FXYD2b with the micelle

The depth of micelle insertion of FXYD2b backbone amide sites is reflected by the Mn^{2+} PRE profile (Fig. 2D). Distance-dependent broadening is observed for peaks from solvent-exposed sites, while residues associated with the hydrophobic regions of the micelle are less or not affected. The data mirror the hydrophobic character of the micelle-associated residues. Addition of MnCl_2 results in substantial line broadening and disappearance of peaks from the N- and C-termini as well as from helix h1. By contrast, peaks from helix h2 retain close to their full intensity in the presence of Mn^{2+} , consistent with the membrane-embedded topology of this segment. The PRE data also mirror the profile of backbone dynamics (Fig. 2B) with micelle-associated sites exhibiting more restricted mobility than water-exposed sites, and water-exposed regions (Pro10–Pro16 and the C-terminus) exhibiting enhanced mobility.

Notably, cross peaks from residues Trp4–Gly7 and Lys55–Arg57 also retain appreciable intensity at high Mn^{2+} concentrations. These sites appear protected from interaction with aqueous Mn^{2+} to a similar extent as Leu29 and Ser50 flanking the transmembrane helix, indicating that they are buried at a similar depth within the micelle. The data effectively restrain the backbone of extracellular Trp4, Tyr5 and Leu6 and cytoplasmic Lys55, Arg56, and Arg57 to the micelle–water interface. The aliphatic side chains of arginines and lysines are frequently found embedded in membranes with their positively charged groups reaching toward the membrane–water interface where they can hydrogen bond with the lipid phosphate head groups [59]. The $^1\text{H}/^{15}\text{N}$ HSQC peak from the indole group of Trp4 also resists complete obliteration by Mn^{2+} , consistent with its insertion in the hydrophobic micelle, and the orientation of the hydrophobic side chain of Leu6 reflects its propensity for membrane insertion.

3.3. Characterization of the arginine side chains

FXYD2b contains seven arginines: Arg3 just before the Trp4–Leu6 micelle-associated segment, Arg25 located after the FYD motif near the extracellular membrane–water interface, Arg46, Arg47 and Arg49 located at the end of the transmembrane helix near the cytoplasmic membrane–water interface, and Arg56 and Arg57 in the micelle-associated region of the C-terminus. All of these may be expected to interact appreciably with the membrane since their backbone amide sites exhibit $^1\text{H}/^{15}\text{N}$ HSQC signals with protection from Mn^{2+} PRE broadening (Fig. 2D).

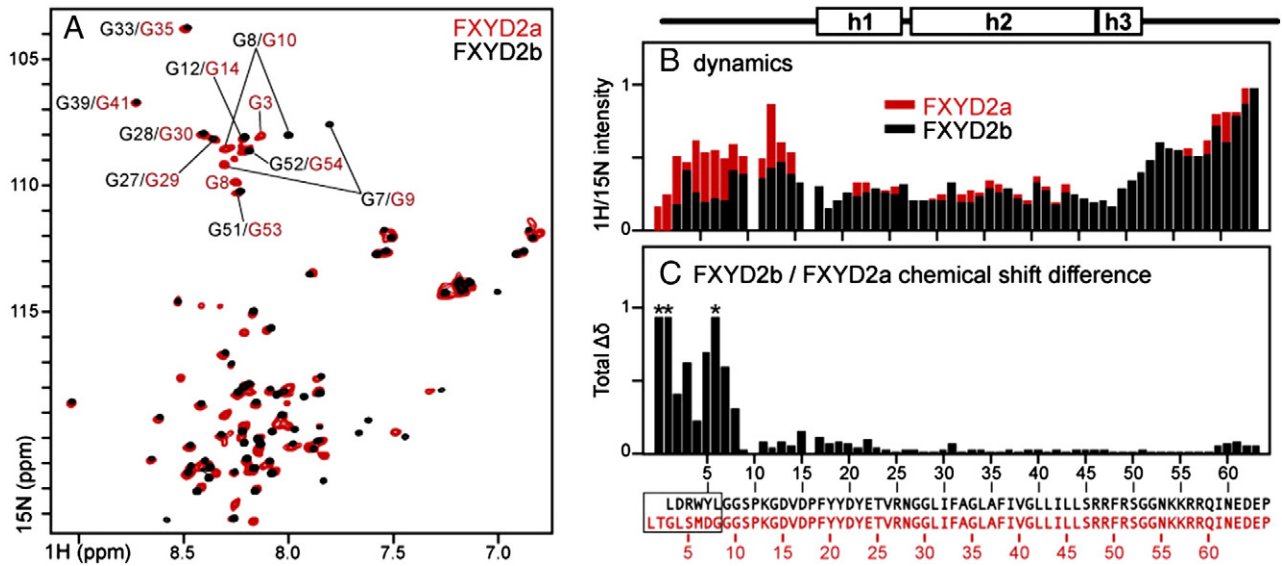


Fig. 3. Comparison between FXYP2b and FXYP2a in micelles. (A) $^1\text{H}/^{15}\text{N}$ HSQC spectra of FXYP2a (red) and FXYP2b (black) in SDS. (B) Normalized $^1\text{H}/^{15}\text{N}$ HSQC peak intensities measured for FXYP2b (black) or FXYP2a (red). (C) Total difference in ^1H and ^{15}N chemical shifts between FXYP2a and FXYP2b ($\Delta\delta_{\text{tot}} = [(\Delta\delta\text{H})^2 + (\Delta\delta\text{N}/5)^2]^{1/2}$). $\Delta\delta\text{N}$ is scaled by 1/5 to account for the 5-fold difference between the chemical shift dispersions of ^{15}N and ^1H . Asterisks denote cross peaks with $\Delta\delta_{\text{tot}} > 1$ ppm. Amino acid sequences and numbers at the bottom correspond to FXYP2b (black) or FXYP2a (red). Differences in the N-termini of the two splice variants are enclosed in the box.

	FXYP	TM
	DPF _{FXYP}	G G F G R R C
A	NP_001265646.1, FXYP1 [human] /3-46	PKEHDPFTYDY-----QSLQIGGLVIAGILFILGILIVLSRRCR-----CKFNE
	NP_001671.2, FXYP2a [human] /13-56	KGDVDPFYDY-----ETVRNGGLIFAGLAFIVGLLILLSRRFR-----CGGNP
	NP_067614.1, FXYP2b [human] /11-54	KGDVDPFYDY-----ETVRNGGLIFAGLAFIVGLLILLSRRFR-----CGGNP
	NP_005962.1, FXYP3 [human] /4-47	EDKNSPFYDWD-----HSLQVGLICAGVLCAMGIIIVMSAKCK-----CKFGP
	NP_001171892.1, FXYP4 [human] /5-48	ANKDPPFYDWD-----KNLQSLGLICGGLLAIAAGIAAVLSGKCK-----CKSSA
	NP_001158077.1, FXYP5 [human] /107-154	FHEDDPFYDE-----HTLRKRGLLVAAVLFITGIIILTSQKCRQLSRLCRNR-
	NP_001158309.1, FXYP6 [human] /6-4	EKEMDPFHYDY-----QTLRIGGLVFAVVLFSVGILLILSRRCK-----CSFNA
	NP_071289.1, FXYP7 [human] /12-55	PEEPDPFYDY-----NTVQTVMGLTATILFLLGILIVISKVK-----CRKAS
	P58550.2, FXYP8 [human] /5-48	EKEIDPFHNY-----QTLRIGGLVFDVVLFLVPSCHLLSHRCK-----CSFNA
	CAD88978.1, FXYP10 [shark] /6-49	PDNDERFTYDY-----YRLRVVGLIIVAIVLIGIILLAGKCR-----CKFNT
B	EH08765.1, DSCAM-like protein-1 [mole rat] /13-56	KGDVDPFHYDY-----ETVRNGGLIFAGLAFVGLLILLSRRFR-----CGGSG
	ELK11872.1, DSCAM-like protein-1 [bat] /24-67	EKEKDPFHYDY-----QTLRIGGLVFAVVLFSVGILLILSRRCK-----CSFNA
	ELK11872.1, DSCAM-like protein-1 [bat] /91-137	KGDVDPFSYDY-----ETVRNGGLIFAALAFVGLIILTRPEDVGT-----SLYFS
	ERE75212.1, TM Ser protease-like [hamster] /581-629	EKEKDPFYDY-----QTLRIGGLVFAVVLFSVGILLILSGSAKGPEDPFHYDF
C	NP_058362.1, R27_p149 [S. enterica Typhi.] /97-147	DYAVEPFYDYS-----GINLYEDGGNFSMASMVYVGPAYYGSFDDVLLQFQNAL
	WP_016240412.1, A1U1_05047 [E. coli] /97-147	DYAVEPFYDY-----GINLYEDGGNFSMASMVYVGPAYYGSFDDVLLQFQNAL
	EOB14608.1, NBO_22g0010 [N. bombycis] /134-187	YFLVDSFYDQRTYNSFLCYLSVLDVNGILFIIDILKFREDLVELGFLT-----CRFKA
D	GAE82117.1, JCM10512 [B. reticulotermitis] /195-213	QQYVNPFYDI-----WTF SKALN-----
	WP_009607332.1, DnaD [Turicibacter] /212-225	PVVDNPFYDWD-----MNE-----
	YP_007850551.1, SugP [C. saccharolyticum] /257-279	AYYLDPFYDYK-----KNVQNLRMYMED-----
	YP_008826316.1, EfmE4452_2428 [E. mundtii] /10-58	VMVDPFYEE-----KNTWVDGLSLFLRFDPFEIDSTTSKSEQTLELSNERY
	WP_021267398.1, lipoprotein [Bacteriovorax] /46-94	LNSVDPFYDYL-----NTLEKDQYDSLREDFVYFADAKYNEFVAVDITYLRTL
	YP_004808764.1, GTP-binding [H. archaeon] /61-111	FDYVDPFYDEL-----ADAIVDVRRLRQALSEVTWASRQIGELRSEYTTKIRNSDA
	WP_022878263.1, polygal [Microbacterium] /383-434	PIDIDPFYDMD-----EGKTPWFTGISIDGLAAVNSPPGAVTRLNGLDGDHPLVLR
	YP_005444950.1, PSMK_08940 [P. mikurensis] /898-946	EHGDDPFYDRL-----HYLPLAQELTGFRIGRAAMPIVAEDGDQVELSTKATGG
	ACO12847.1, CutP7 [Lepeophtheirus salmonis] /20-68	TALSDPFYDYL-----NYDSYNNQERPYITPPRYIPEQNPPVYAPIPEQAPIN
	XP_007422682.1, pet1 [Python] /41-91	RLDVPDLYYEP-----GAIYTVSVTGAEKATSVILQIVPPENSSGGSWEHEHQTIK
	WP_008858653.1, T3resR [D. succinatophilus] /433-481	WEKMDPFYDMD-----IIVDFHHAAGKGYQLLTWFHPIKLLGLTATPERMDH
	XP_005635989.1, ankyrin repeat MYND [dog] /237-285	HEGEDPFYDY-----KRFLDDDLTLPEMYIYSTDNHSLPVTCSFRKELDAV
	WP_009597733.1, TonB-linked OMP [Alistipes] /396-444	FTPLDPFYDD-----EQTMHYTKDDNTGIVNPLAMIDKDANGYQSLISRWFQF
	XP_001524766.1, LELG [L. elongisporus] /949-997	GEKVNPFYDE-----KHKRWLDRTPKIEEQLNAGKAPPPPPSMKKKPGASAAA
	EES52221.1, HAS [L. ferrodiazotrophum] /553-601	SSPVNPFYDYL-----QGQNYITNGQVGFATPKYSMTLGTVDQYIIGGTG

Fig. 4. Amino acid sequence alignment of FXYP homology domains. (A) FXYP family proteins. (B–D) Proteins obtained by BLAST search of the NCBI database against the DVPDPPYD polypeptide sequence. (B) Membrane proteins containing entire FXYP protein sequences, including conserved FXYP and transmembrane (TM) motifs. The Down syndrome cell adhesion molecule-like protein (DSCAM, ELK11872) contains two FXYP protein sequences, from residues 24–67 and residues 91–137. (C) Other membrane proteins with a FXYP motif preceding a TM sequence. (D) Soluble protein sequences with a conserved FXYP motif. Alignments were generated with ClustalW [57] in Jalview [58], and rendered with ClustalW coloring. Transmembrane sequences were identified with TMHMM [56]. FASTA-formatted alignments are provided in Supporting materials.

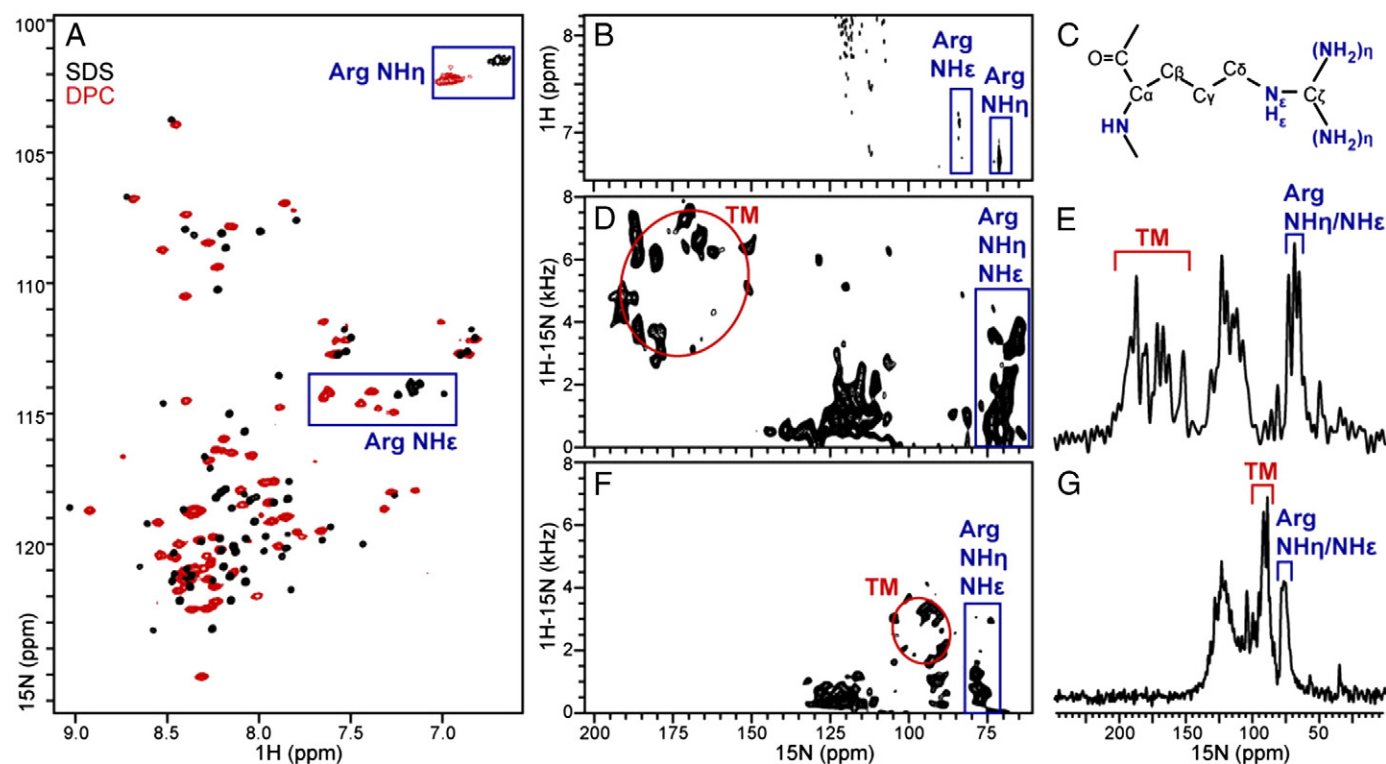


Fig. 5. Solution and solid-state NMR spectra of uniformly ^{15}N labeled FXYP2b in detergent micelles and phospholipid bilayers. (A, B) Solution NMR $^1\text{H}/^{15}\text{N}$ HSQC spectra in SDS (black) and DPC (red) micelles. Peaks from the seven arginine guanidinium groups are enclosed in blue boxes. (A) The ^{15}N frequencies from Arg side chains peaks are not actual but reflect the reduced ^{15}N spectral width used to measure the spectra. (B) The spectrum was obtained with full ^{15}N spectral width to observe the correct ^1H and ^{15}N frequencies of peaks from arginine guanidinium NH sites. (C) Molecular structure of arginine. (D–G) One- and two-dimensional $^1\text{H}/^{15}\text{N}$ OS solid-state NMR spectra spectra of FXYP2b in lipid bilayers aligned with the membrane perpendicular (D, E) or parallel (F, G) to the magnetic field. Peaks from the transmembrane helix (TM) trace wheel-like patterns (red circles). Peaks assigned to arginine guanidinium NH groups are enclosed in blue boxes.

The HSQC spectra of FXYP2b in micelles display a broad arginine guanidinium NH signal intensity, consistent with intermediate rotational dynamics of the Arg side chains at this temperature (Fig. 5A). In the spectra of FXYP2b in SDS, cross peaks from arginine guanidinium NH groups are clustered in a region between 7.0 and 7.2 ppm (Fig. 5A; black). However, the spectra obtained for the protein in DPC exhibit six well-resolved NH cross peaks between 7.2 and 7.7 ppm (Fig. 5A; red). Two of these peaks appear significantly shifted downfield, as might be expected for hydrogen-bonded guanidinium groups [60, 61], suggesting that these arginine side chains interact with the DPC phosphates. This result is substantiated by the solid-state NMR spectra obtained for uniformly ^{15}N -labeled FXYP2b in magnetically aligned phospholipid bilayers (Fig. 5D–G), where significant resonance intensity is observed at ^{15}N frequencies (70–90 ppm) associated with arginine side chains [60–62].

The one-dimensional cross polarization (CP) spectra and the two-dimensional $^1\text{H}/^{15}\text{N}$ separated local field (SLF) spectra exhibit remarkable resolution. Resonances from amide sites in the transmembrane helix (TM) conform to wheel-like patterns in the spectral regions expected for an α -helix crossing the membrane at an angle of $\sim 20^\circ$ [63, 64], with ^{15}N frequencies of 150–200 ppm in the spectra from bilayers aligned perpendicular to magnetic field (Fig. 5D, E), or 85–100 ppm in the spectra from parallel membranes (Fig. 5F, G). For both membrane alignments, peaks in the central region of the ^{15}N spectrum (100–130 ppm) are assigned to sites with sufficient mobility to cause isotropic averaging of the ^{15}N chemical shift and ^1H – ^{15}N dipolar coupling, as might be expected for the non-helical regions of the protein.

In the case of fully rigid guanidinium groups, each of the seven arginines in FXYP2b would be expected to contribute three peaks to the solution and solid-state NMR spectra, one from NH and two from NH_2 groups. However, in the absence of hydrogen bonding or other

immobilizing influences, rapid flip rates around the N_ϵ – C_ζ bond average the NH_2 NMR signals [60,61]. Resonance overlap in the solid-state NMR spectra of FXYP2b precludes identification of the number of peaks from arginine side chains. However, since these signals display observable ^1H – ^{15}N dipolar couplings in the SLF spectra, we infer that they must emanate from sites that do not undergo rapid isotropic reorientation.

Notably, both the ^1H – ^{15}N dipolar couplings and the ^{15}N chemical shift frequencies of these peaks change with the overall magnetic alignment of the lipid bilayer membrane in the magnetic field, indicating that the Arg side chains themselves adopt preferred orientations relative to the lipid bilayer. Since FXYP2b contains no other N-bearing side chains that would resonate in this region of the spectrum, we conclude that at least some of the arginine side chains are sufficiently immobilized to yield orientation-dependent solid-state NMR signals. Such immobilization could result from hydrogen bond formation between arginine side chains and the lipid phosphate or polar head groups.

3.4. Implications for function

The crystal structures of pig kidney Na,K-ATPase highlight a highly electropositive region near the cytoplasmic membrane surface and the Na^+/K^+ ion binding sites of the α subunit. This region is composed of arginine and lysine residues located at the cytoplasmic ends and connecting loops of the α subunit's transmembrane helices, including three arginines that were proposed to constitute a voltage-sensing module [29]. To examine the location of FXYP2 arginines in the context of the Na,K-ATPase, we generated a model of the α/β /FXYP2b complex by replacing the coordinates of the transmembrane helix of endogenous FXYP2 in the recent crystal structure of Na,K-ATPase from pig kidney [34] with those of full-length FXYP2b determined by NMR in this

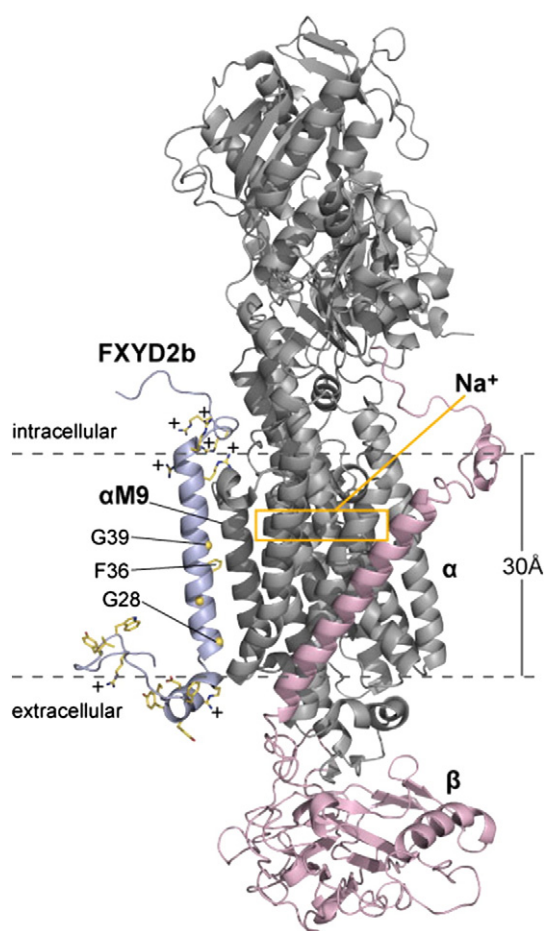


Fig. 6. Structural model of the α/β /FXYD2b complex. The model was generated by replacing the coordinates of the transmembrane helix of endogenous FXYD2 in the crystal structure of Na,K-ATPase from pig kidney [34] with those of full-length FXYD2b determined by NMR. FXYD2b (light blue) associates with helix M9 of the α subunit (gray). FXYD2b arginine and lysine side chains contribute significant positive charge (+) to the cytoplasmic membrane surface. The FXYD2b spanning helix rests on the extracellular membrane surface near but without contacting the β subunit (pink). The yellow box marks the location of the intramembrane binding sites for Na^+ .

study (Fig. 6). The model shows that the membrane surface location of Arg and Lys in FXYD2b could significantly contribute to the effective electrostatic potential near the Na,K-ATPase's Na^+ binding sites.

Molecular dynamics simulations indicate that specific arginine side chains in channel voltage sensors can pair with one or more lipid phosphodiester groups at the membrane–water interface, dramatically influencing the local electric field [65]. This is consistent with the requirement of negatively charged lipid phosphodiester groups for channel function [66] and has provided an attractive explanation for the voltage sensor mechanism. Similar requirements for negatively charged phospholipids have been reported for optimal activity of the Na,K-ATPase activity (see [67,68] and references therein).

Our data show that several arginines of FXYD2b appear to associate with the lipid bilayer interfacial regions. In the presence of phospholipids, they are sufficiently immobilized to yield both orientation-dependent solid-state NMR signals as well as shifted solution NMR signals. Their strategic positions in the structure of FXYD2b allows their guanidinium groups to form hydrogen bonds with the phosphate and polar head groups of membrane phospholipids, interactions that could be particularly significant in the presence of negatively charged lipids such as phosphatidylserine. This property could be important for the recruitment of specific phospholipids near the Na,K-ATPase, providing one potential explanation for the Na,K-ATPase stabilizing effect of FXYD proteins [54,55], as well as for regulating the enzyme's activity.

Acknowledgements

This research was supported by grants from the National Institutes of Health (GM100265; AI074805; CA082864). The NMR studies utilized the NMR Facility at Sanford-Burnham Medical Research Institute, and the Resource for Molecular Imaging of Proteins at UCSD, each supported by grants from the National Institutes of Health (P30 CA030199; P41 EB002031).

Appendix A. Supplementary data

Supplementary data to this article can be found online at <http://dx.doi.org/10.1016/j.bbamm.2014.04.021>.

References

- [1] F. Cornelius, Y.A. Mahmmoud, Functional modulation of the sodium pump: the regulatory proteins "Fixit", *News Physiol. Sci.* 18 (2003) 119–124.
- [2] H. Garty, S.J. Karlish, Role of FXYD proteins in ion transport, *Annu. Rev. Physiol.* 68 (2006) 431–459.
- [3] K. Geering, FXYD proteins: new regulators of Na,K-ATPase, *Am. J. Physiol. Renal Physiol.* 290 (2006) F241–F250.
- [4] G. Blanco, R.W. Mercer, Isozymes of the Na,K-ATPase: heterogeneity in structure, diversity in function, *Am. J. Physiol.* 275 (1998) F633–F650.
- [5] K.J. Sweadner, E. Rael, The FXYD gene family of small ion transport regulators or channels: cDNA sequence, protein signature sequence, and expression, *Genomics* 68 (2000) 41–56.
- [6] K. Pihakaski-Maunsbach, H. Vorum, E.M. Locke, H. Garty, S.J. Karlish, A.B. Maunsbach, Immunocytochemical localization of Na,K-ATPase gamma subunit and CHIF in inner medulla of rat kidney, *Ann. N. Y. Acad. Sci.* 986 (2003) 401–409.
- [7] M.J. Shattock, Phospholemman: its role in normal cardiac physiology and potential as a druggable target in disease, *Curr. Opin. Pharmacol.* 9 (2009) 160–166.
- [8] I.C. Meij, J.B. Koenderink, H. van Bokhoven, K.F. Assink, W.T. Groenestege, J.J. de Pont, R.J. Bindels, L.A. Monnens, L.P. van den Heuvel, N.V. Knoers, Dominant isolated renal magnesium loss is caused by misrouting of the Na^+ , K^+ -ATPase gamma-subunit, *Nat. Genet.* 26 (2000) 265–266.
- [9] B.W. Morrison, J.R. Moorman, G.C. Kowdley, Y.M. Kobayashi, L.R. Jones, P. Leder, Mat-8, a novel phospholemman-like protein expressed in human breast tumors, induces a chloride conductance in *Xenopus* oocytes, *J. Biol. Chem.* 270 (1995) 2176–2182.
- [10] J.S. Nam, S. Hirohashi, L.M. Wakefield, Dysadherin: a new player in cancer progression, *Cancer Lett.* 255 (2007) 161–169.
- [11] K. Choudhury, A. McQuillin, V. Puri, J. Pimm, S. Datta, S. Thirumalai, R. Krasucki, J. Lawrence, N.J. Bass, D. Quested, C. Crombie, G. Fraser, N. Walker, H. Nadeem, S. Johnson, D. Curtis, D. St Clair, H.M. Gurling, A genetic association study of chromosome 11q22–24 in two different samples implicates the FXYD6 gene, encoding phospholipopolin, in susceptibility to schizophrenia, *Am. J. Hum. Genet.* 80 (2007) 664–672.
- [12] C.M. Franzin, J. Yu, K. Thai, J. Choi, F.M. Marassi, Correlation of gene and protein structures in the FXYD family proteins, *J. Mol. Biol.* 354 (2005) 743–750.
- [13] B. Forbush III, J.H. Kaplan, J.F. Hoffman, Characterization of a new photoaffinity derivative of ouabain: labeling of the large polypeptide and of a proteolipid component of the Na,K-ATPase, *Biochemistry* 17 (1978) 3667–3676.
- [14] J.H. Collins, J. Leszyk, The "gamma subunit" of Na,K-ATPase: a small, amphiphilic protein with a unique amino acid sequence, *Biochemistry* 26 (1987) 8665–8668.
- [15] P. Beguin, X. Wang, D. Firsov, A. Puoti, D. Claeys, J.D. Horisberger, K. Geering, The gamma subunit is a specific component of the Na,K-ATPase and modulates its transport function, *EMBO J.* 16 (1997) 4250–4260.
- [16] E. Arystarkhova, R.K. Wetzel, N.K. Asinowski, K.J. Sweadner, The gamma subunit modulates Na^+ and K^+ affinity of the renal Na,K-ATPase, *J. Biol. Chem.* 274 (1999) 33183–33185.
- [17] H.X. Pu, F. Cluzeaud, R. Goldshleger, S.J. Karlish, N. Farman, R. Blostein, Functional role and immunocytochemical localization of the gamma a and gamma b forms of the Na,K-ATPase gamma subunit, *J. Biol. Chem.* 276 (2001) 20370–20378.
- [18] E. Arystarkhova, C. Donnet, N.K. Asinowski, K.J. Sweadner, Differential regulation of renal Na,K-ATPase by splice variants of the gamma subunit, *J. Biol. Chem.* 277 (2002) 10162–10172.
- [19] D.H. Jones, T.Y. Li, E. Arystarkhova, K.J. Barr, R.K. Wetzel, J. Peng, K. Markham, K.J. Sweadner, G.H. Fong, G.M. Kidder, Na,K-ATPase from mice lacking the gamma subunit (FXYD2) exhibits altered Na^+ affinity and decreased thermal stability, *J. Biol. Chem.* 280 (2005) 19003–19011.
- [20] A. Zouzoulas, P.B. Dunham, R. Blostein, The effect of the gamma modulator on Na/K pump activity of intact mammalian cells, *J. Membr. Biol.* 204 (2005) 49–56.
- [21] K.J. Sweadner, J.L. Pascoa, C.A. Salazar, E. Arystarkhova, Post-transcriptional control of Na,K-ATPase activity and cell growth by a splice variant of FXYD2 protein with modified mRNA, *J. Biol. Chem.* 286 (2011) 18290–18300.
- [22] B. Kuster, A. Shainskaya, H.X. Pu, R. Goldshleger, R. Blostein, M. Mann, S.J. Karlish, A new variant of the gamma subunit of renal Na,K-ATPase. Identification by mass spectrometry, antibody binding, and expression in cultured cells, *J. Biol. Chem.* 275 (2000) 18441–18446.

- [23] E. Arystarkhova, R.K. Wetzel, K.J. Sweadner, Distribution and oligomeric association of splice forms of Na(+)-K(+)-ATPase regulatory gamma-subunit in rat kidney, *Am. J. Physiol. Renal Physiol.* 282 (2002) F393–F407.
- [24] R.W. Mercer, D. Biemesderfer, D.P. Bliss Jr., J.H. Collins, B. Forbush III, Molecular cloning and immunological characterization of the gamma polypeptide, a small protein associated with the Na, K-ATPase, *J. Cell Biol.* 121 (1993) 579–586.
- [25] H.X. Pu, R. Scanzano, R. Blostein, Distinct regulatory effects of the Na, K-ATPase gamma subunit, *J. Biol. Chem.* 277 (2002) 20270–20276.
- [26] K. Pihakaski-Maunsbach, H. Vorum, B. Honore, S. Tokonabe, J. Frokiaer, H. Garty, S.J. Karlsh, A.B. Maunsbach, Locations, abundances, and possible functions of FXYP ion transport regulators in rat renal medulla, *Am. J. Physiol. Renal Physiol.* 291 (2006) F1033–F1044.
- [27] D.H. Jones, T.C. Davies, G.M. Kidder, Embryonic expression of the putative gamma subunit of the sodium pump is required for acquisition of fluid transport capacity during mouse blastocyst development, *J. Cell Biol.* 139 (1997) 1545–1552.
- [28] M. Lindzen, R. Aizman, Y. Lifshitz, I. Lubarski, S.J. Karlsh, H. Garty, Structure-function relations of interactions between Na, K-ATPase, the gamma subunit, and corticosteroid hormone-induced factor, *J. Biol. Chem.* 278 (2003) 18738–18743.
- [29] J.P. Morth, B.P. Pedersen, M.S. Toustrup-Jensen, T.L. Sorensen, J. Petersen, J.P. Andersen, B. Vilsen, P. Nissen, Crystal structure of the sodium-potassium pump, *Nature* 450 (2007) 1043–1049.
- [30] P. Teriete, C.M. Franzin, J. Choi, F.M. Marassi, Structure of the Na, K-ATPase regulatory protein FXYP1 in micelles, *Biochemistry* 46 (2007) 6774–6783.
- [31] L. Yatime, M. Laursen, J.P. Morth, M. Esmann, P. Nissen, N.U. Fedosova, Structural insights into the high affinity binding of cardiotonic steroids to the Na+, K+-ATPase, *J. Struct. Biol.* 174 (2011) 296–306.
- [32] M. Laursen, L. Yatime, P. Nissen, N.U. Fedosova, Crystal structure of the high-affinity Na+ K+-ATPase-ouabain complex with Mg2+ bound in the cation binding site, *Proc. Natl. Acad. Sci. U. S. A.* 110 (2013) 10958–10963.
- [33] M. Nyblom, H. Poulsen, P. Gourdon, L. Reinhard, M. Andersson, E. Lindahl, N. Fedosova, P. Nissen, Crystal structure of Na+, K(+)-ATPase in the Na(+)-bound state, *Science* 342 (2013) 123–127.
- [34] R. Kanai, H. Ogawa, B. Vilsen, F. Cornelius, C. Toyoshima, Crystal structure of a Na+—bound Na+, K+—ATPase preceding the E1P state, *Nature* 502 (2013) 201–206.
- [35] H. Ogawa, T. Shinoda, F. Cornelius, C. Toyoshima, Crystal structure of the sodium-potassium pump (Na+, K+-ATPase) with bound potassium and ouabain, *Proc. Natl. Acad. Sci. U. S. A.* 106 (2009) 13742–13747.
- [36] T. Shinoda, H. Ogawa, F. Cornelius, C. Toyoshima, Crystal structure of the sodium-potassium pump at 2.4 Å resolution, *Nature* 459 (2009) 446–450.
- [37] C.M. Franzin, P. Teriete, F.M. Marassi, Structural similarity of a membrane protein in micelles and membranes, *J. Am. Chem. Soc.* 129 (2007) 8078–8079.
- [38] P. Teriete, K. Thai, J. Choi, F.M. Marassi, Effects of PKA phosphorylation on the conformation of the Na, K-ATPase regulatory protein FXYP1, *Biochim. Biophys. Acta* 1788 (2009) 2462–2470.
- [39] K.J. Crowell, C.M. Franzin, A. Koltay, S. Lee, A.M. Lucchese, B.C. Snyder, F.M. Marassi, Expression and characterization of the FXYP ion transport regulators for NMR structural studies in lipid micelles and lipid bilayers, *Biochim. Biophys. Acta* 1645 (2003) 15–21.
- [40] F. Delaglio, S. Grzesiek, G.W. Vuister, G. Zhu, J. Pfeifer, A. Bax, NMRPipe: a multidimensional spectral processing system based on UNIX pipes, *J. Biomol. NMR* 6 (1995) 277–293.
- [41] T.D. Goddard, D.G. Kneller, SPARKY 3, University of California, San Francisco, 2004.
- [42] J. Cavanagh, W.J. Fairbrother, A.G. Palmer, N.J. Skelton, *Protein NMR Spectroscopy: Principles and Practice*, Academic Press, San Diego, 1996.
- [43] Y. Shen, F. Delaglio, G. Cornilescu, A. Bax, TALOS+: a hybrid method for predicting protein backbone torsion angles from NMR chemical shifts, *J. Biomol. NMR* 44 (2009) 213–223.
- [44] R. Mahalakshmi, F.M. Marassi, Orientation of the *Escherichia coli* outer membrane protein OmpX in phospholipid bilayer membranes determined by solid-state NMR, *Biochemistry* 47 (2008) 6531–6538.
- [45] C.D. Schwieters, J.J. Kuszewski, N. Tjandra, G.M. Clore, The Xplor-NIH NMR molecular structure determination package, *J. Magn. Reson.* 160 (2003) 65–73.
- [46] C.D. Schwieters, J.J. Kuszewski, G. Marius Clore, Using Xplor-NIH for NMR molecular structure determination, *Prog. Nucl. Magn. Reson. Spectrosc.* 48 (2006) 47–62.
- [47] G.A. Bermejo, G.M. Clore, C.D. Schwieters, Smooth statistical torsion angle potential derived from a large conformational database via adaptive kernel density estimation improves the quality of NMR protein structures, *Protein Sci.* 21 (2012) 1824–1836.
- [48] C. Xu, E. Gagnon, M.E. Call, J.R. Schnell, C.D. Schwieters, C.V. Carman, J.J. Chou, K.W. Wucherpfennig, Regulation of T cell receptor activation by dynamic membrane binding of the CD3epsilon cytoplasmic tyrosine-based motif, *Cell* 135 (2008) 702–713.
- [49] R.A. Laskowski, J.A. Rullmann, M.W. MacArthur, R. Kaptein, J.M. Thornton, AQUA and PROCHECK-NMR: programs for checking the quality of protein structures solved by NMR, *J. Biomol. NMR* 8 (1996) 477–486.
- [50] K.J. Wypijewski, J. Howie, L. Reilly, L.B. Tulloch, K.L. Aughton, L.M. McLatchie, M.J. Shattock, S.C. Calaghan, W. Fuller, A separate pool of cardiac phospholemman that does not regulate or associate with the sodium pump: multimers of phospholemman in ventricular muscle, *J. Biol. Chem.* 288 (2013) 13808–13820.
- [51] X.Q. Zhang, J. Wang, L.L. Carl, J. Song, B.A. Ahlers, J.Y. Cheung, Phospholemman regulates cardiac Na+/Ca2+ exchanger by interacting with the exchanger's proximal linker domain, *Am J Physiol Cell Physiol* 296 (2009) C911–921.
- [52] X. Wang, G. Gao, K. Guo, V. Yarotsky, C. Huang, K.S. Elmslie, B.Z. Peterson, Phospholemman modulates the gating of cardiac L-type calcium channels, *Biophys. J.* 98 (2010) 1149–1159.
- [53] C.M. Franzin, X.M. Gong, P. Teriete, F.M. Marassi, Structures of the FXYP regulatory proteins in lipid micelles and membranes, *J. Bioenerg. Biomembr.* 39 (2007) 379–383.
- [54] N.K. Mishra, Y. Peleg, E. Cirri, T. Belogus, Y. Lifshitz, D.R. Voelker, H.J. Apell, H. Garty, S.J. Karlsh, FXYP proteins stabilize Na, K-ATPase: amplification of specific phosphatidylserine-protein interactions, *J. Biol. Chem.* 286 (2011) 9699–9712.
- [55] P. Beguin, G. Crambert, S. Guennoun, H. Garty, J.D. Horisberger, K. Geering, CHIF, a member of the FXYP protein family, is a regulator of Na, K-ATPase distinct from the gamma-subunit, *EMBO J.* 20 (2001) 3993–4002.
- [56] A. Krogh, B. Larsson, G. von Heijne, E.L. Sonnhammer, Predicting transmembrane protein topology with a hidden Markov model: application to complete genomes, *J. Mol. Biol.* 305 (2001) 567–580.
- [57] J.D. Thompson, D.G. Higgins, T.J. Gibson, CLUSTAL W: improving the sensitivity of progressive multiple sequence alignment through sequence weighting, position-specific gap penalties and weight matrix choice, *Nucleic Acids Res.* 22 (1994) 4673–4680.
- [58] M. Clamp, J. Cuff, S.M. Searle, G.J. Barton, The Jalview Java alignment editor, *Bioinformatics* 20 (2004) 426–427.
- [59] E.V. Schow, J.A. Freites, P. Cheng, A. Bernsel, G. von Heijne, S.H. White, D.J. Tobias, Arginine in membranes: the connection between molecular dynamics simulations and translocon-mediated insertion experiments, *J. Membr. Biol.* 239 (2011) 35–48.
- [60] S.M. Pascal, T. Yamazaki, A.U. Singer, L.E. Kay, J.D. Forman-Kay, Structural and dynamic characterization of the phosphotyrosine binding region of a Src homology 2 domain-phosphopeptide complex by NMR relaxation, proton exchange, and chemical shift approaches, *Biochemistry* 34 (1995) 11353–11362.
- [61] G.D. Henry, B.D. Sykes, Determination of the rotational dynamics and pH dependence of the hydrogen exchange rates of the arginine guanidino group using NMR spectroscopy, *J. Biomol. NMR* 6 (1995) 59–66.
- [62] A.T. Petkova, J.G. Hu, M. Bizounok, M. Simpson, R.G. Griffin, J. Herzfeld, Arginine activity in the proton-motive photocycle of bacteriorhodopsin: solid-state NMR studies of the wild-type and D85N proteins, *Biochemistry* 38 (1999) 1562–1572.
- [63] F.M. Marassi, S.J. Opella, A solid-state NMR index of helical membrane protein structure and topology, *J. Magn. Reson.* 144 (2000) 150–155.
- [64] J. Wang, J. Denny, C. Tian, S. Kim, Y. Mo, F. Kovacs, Z. Song, K. Nishimura, Z. Gan, R. Fu, J.R. Quine, T.A. Cross, Imaging membrane protein helical wheels, *J. Magn. Reson.* 144 (2000) 162–167.
- [65] V. Jogini, B. Roux, Dynamics of the Kv1.2 voltage-gated K+ channel in a membrane environment, *Biophys. J.* 93 (2007) 3070–3082.
- [66] D. Schmidt, Q.X. Jiang, R. MacKinnon, Phospholipids and the origin of cationic gating charges in voltage sensors, *Nature* 444 (2006) 775–779.
- [67] F. Cornelius, Y.A. Mahmoud, Modulation of FXYP interaction with Na, K-ATPase by anionic phospholipids and protein kinase phosphorylation, *Biochemistry* 46 (2007) 2371–2379.
- [68] Y. Lifshitz, E. Petrovich, H. Haviv, R. Goldshleger, D.M. Tal, H. Garty, S.J. Karlsh, Purification of the human alpha2 isoform of Na, K-ATPase expressed in *Pichia pastoris*. Stabilization by lipids and FXYP1, *Biochemistry* 46 (2007) 14937–14950.